

Temperature-dependent Transport and Thermal-diffusion Effects on Diffusion Flames

Joseph E. Hibdon Jr^{a,*}, Moshe Matalon^b

^a*Mathematics Department, Northeastern Illinois University, Chicago, IL 60625*

^b*Mechanical Science and Engineering, University of Illinois at Urbana-Champaign, Urbana, IL 61801*

Abstract

In this paper we examine the effects of temperature-dependent transport and thermal diffusion on the structure and characteristics of a diffusion flame. The configuration adopted is the planar unstrained flame with a bulk flow directed toward the reaction zone from either the fuel or the oxidizer sides. Included in this discussion is the no-flow case, where the reactants reach the reaction zone purely by diffusion. The model allows for non-unity and distinct Lewis numbers, for the fuel and oxidizer. Results show that the variations of the thermal conductivity and the diffusion coefficients with temperature affect the flame standoff distance and flame temperature and the profiles of temperature and concentration, in accord with experimental data. The predicted extinction conditions are exhibited by a critical Damköhler number \mathbb{D}_c below which the flame extinguishes. This \mathbb{D}_c is significantly smaller for the temperature dependent case when compared with previous analysis without the temperature dependence. Thermal diffusion, also known as the Soret effect, also affects the flame standoff distance by shifting it towards the fuel/oxidizer and affects the flame temperature by making it smaller/larger for heavy/light fuels respectively. Predicted extinctions \mathbb{D}_c are minimally affected by the Soret effects, except when having very heavy fuels. The amount of leakage across the reaction sheet that causes extinction is more/less for light/heavy fuels, respectively.

Keywords: Diffusion Flame, Soret Effect, Extinction, Temperature-dependent Transport

1. Introduction

Analytical studies of diffusion flames directed towards understanding their fundamental properties, have typically assumed constant transport properties [1–5]. It is known, however, that the thermal conductivity of the mixture and the molecular diffusivities of the various species are strongly dependent on temperature, which have non-trivial consequences on the flame characteristics that need to be properly examined.

*Corresponding author; current address: Northeastern Illinois University

Email addresses: j-hibdonjr@neiu.edu (Joseph E. Hibdon Jr), matalon@illinois.edu (Moshe Matalon)

Indeed, the dependence of transport properties on temperature has been accounted for in numerical studies in order to properly simulate the diffusion fluxes and enable a more accurate comparison with experiments. For example, accounting for these effects Law and Law [6] compared quantitatively the properties of heptane droplet combustion with experimental data, and Puri and Libby [7] provided an assessment of the effect of water gas-shift equilibrium on the flame. Fundamental understanding of the properties of diffusion flames, obtained by comparing their structure for constant and temperature-dependent transport, has not been previously reported.

Another effect that has been typically neglected in theoretical studies is thermal diffusion, or Soret effect, which correspond to the diffusion of mass caused by temperature gradients. Cross-transport are typically considered second order effects and have been often neglected in combustion studies; c.f. Warnatz et al. [8]. Recently, Rosner [9] pointed out that thermal diffusion could have a nontrivial effect on flame characteristics, particularly in combustible mixtures in which the molecular diffusivities of the fuel and oxidizer are very different than the thermal diffusivity of the mixture, i.e., in mixtures in which the Lewis numbers are significantly different than one; see also Rosner et al. [10]. In a follow-up study Arias-Zugasti and Rosner [11] examined the influence of thermal diffusion on the temperature and standoff distance of a counterflow diffusion flame, accounting also for temperature dependent transport, but restricting attention to the Burke-Shumann limit of complete combustion.

The objective of this work is to provide a fundamental understanding of transport and cross-transport effects on the structure of diffusion flames. The adopted configuration is the simplest planar unstrained diffusion flame, where a bulk uniform flow containing fuel is directed towards the reaction zone with the oxidizer diffusing against the stream, and the reverse situation in which oxidizer is supplied in the inflow and fuel is diffusing against the flow towards the reaction zone. Included in the discussion is the idealized limit of no flow, where the reactants reach the reaction zone purely by diffusion. The analysis follows the asymptotic formulation of Cheatham and Matalon [5], extended appropriately to accommodate for temperature-dependent transport coefficients and diffusion fluxes that result from the Soret effect. For steady planar flames, as discussed here, the formulation is valid for *non-unity* and *distinct Lewis numbers* for the fuel and oxidizer, and allows for finite-rate chemistry, covering the entire range of Damköhler numbers from the Burke-Schumann limit of complete combustion down to extinction.

We note for clarity that for *multi-dimensional* and *time-dependent* problems the general theory presented in Cheatham and Matalon [5] is limited to equi-diffusion flames, i.e., flames for which the Lewis numbers do not significantly differ from one. For otherwise, the temperature along the reaction sheet varies by $O(1)$ amounts from its stoichiometric value, changes that cannot be properly captured by the asymptotic analysis. Unfortunately, this fact was not explicitly stated in the referenced paper. Possible confusion stems also from the inappropriate use of the term “adiabatic flame temperature”, which intended to designate *the stoichiometric temperature*, namely the temperature along the stoichiometric surface where both, the fuel and oxidizer are completely consumed. Evidently, the stoichiometric temperature depends on the means by which fuel and oxidizer are transported to the stoichiometric surface (or reaction sheet), namely on their molecular diffusivities or Lewis numbers, as explicitly stated

in the referenced paper and shown for the planar chambered flame considered therein. The statement in Cheatham and Matalon [5] on page 112 that “to leading order ... the temperature along the sheet is the adiabatic flame temperature, assumed constant” did not mean constant for all Lewis numbers, but rather constant along the reaction sheet, for given Lewis numbers.

In the next section, the flow configuration is described along with the governing equations and the asymptotic formulation. The effects of variable transport are discussed in Sec. 3 and the effects of thermal-diffusion are discussed in Sec. 4. The presented results illustrate the effects of the various parameters on the flame structure, and provide expressions for the flame standoff distance and flame temperature, as well as explicit conditions for flame extinction.

2. Formulation

A schematic of the chambered-diffusion flame configuration is shown in Fig. 1. Fuel is supplied in a stream flowing from the bottom of the chamber, assumed at $\tilde{x} = -L$, and oxidizer diffuses inwards from the top boundary, $\tilde{x} = L$. The reverse but equivalent problem, in which oxidizer is supplied in the stream and fuel diffuses against it, is readily available by exchanging the roles played by the two reactants. The mass flux \tilde{m} at the inflow is specified, and the flow is assumed to remain uniform across the chamber. Conditions at the two boundaries are maintained uniform, such that

$$\begin{aligned} \tilde{T} &= \tilde{T}_0, \quad \tilde{\rho} = \tilde{\rho}_0, \quad \tilde{Y}_F = \tilde{Y}_{F_0}, \quad \tilde{Y}_O = 0 & \text{at } \tilde{x} = -L \\ \tilde{T} &= \tilde{T}_1, \quad \tilde{\rho} = \tilde{\rho}_1, \quad \tilde{Y}_F = 0, \quad \tilde{Y}_O = \tilde{Y}_{O_1} & \text{at } \tilde{x} = L, \end{aligned}$$

where \tilde{T} and $\tilde{\rho}$ stand for the temperature and density of the mixture, \tilde{Y}_F and \tilde{Y}_O are the mass fractions of the fuel and oxidizer, and the subscripts 0 and 1 denote conditions at the bottom/top of the chamber, respectively.

Maintaining uniform conditions at the boundaries is experimentally challenging because of the difficulty of supplying the reactants and removing the combustion products uniformly across the entire cross-section of the chamber. An experimental configuration capable of overcoming these difficulties, and generating a flat one-dimensional nearly-unstrained diffusion flame, was first introduced at EPFL by P. Monkewitz. The realization of the boundary conditions at the top of the chamber was demonstrated by Lo Jacono et al. [12] by introducing the oxidizer into the chamber through an array of hundreds of closely spaced hypodermic needles, separated equally from each other to allow the hot combustion products to escape between them. The inhomogeneity near the exit plane of the needles was limited to a thin layer of thickness comparable to the needle spacing, such that uniform conditions prevailed just below this layer, a location identified as the virtual boundary. An improved design was subsequently developed by Robert and Monkewitz [13, 14] where both reactants were introduced into the chamber through array of needles. The implementation of this design produced flat flames that experienced very little residual strain, caused primarily by temperature inhomogeneities in the supply and exhaust paths. It also permitted better control of the magnitude and direction of the bulk flow with provisions to reach the limiting situation

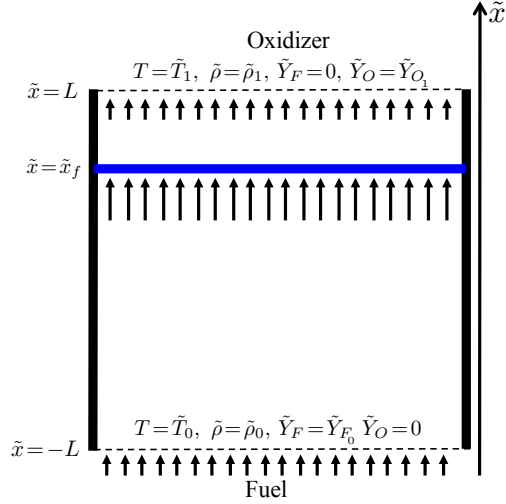


Figure 1: Schematic of the chambered-flame configuration shown for $\tilde{m} > 0$, i.e., when the fuel is supplied in the incoming stream and the oxidizer is diffusing against the stream; the reverse situation with $\tilde{m} < 0$ corresponds to oxidizer supplied in the stream and fuel diffusing against the stream.

of a “pure diffusion flame” corresponding to $\tilde{m} = 0$, namely when the fuel and oxidizer reach the reaction zone from opposing ends solely by diffusion with no net flow across the flame.

The chemical activity in the chamber is modeled by a global one-step irreversible reaction of the form



where ν_F, ν_O are the stoichiometric coefficients of the fuel and oxidizer, respectively, and Q is the total heat released during combustion. The reaction rate $\tilde{\omega}$ is assumed to obey an Arrhenius law with a pre-exponential factor \mathcal{B} and overall activation energy E , namely

$$\tilde{\omega} = \mathcal{B} \left(\frac{\tilde{\rho} \tilde{Y}_F}{W_F} \right) \left(\frac{\tilde{\rho} \tilde{Y}_O}{W_O} \right) e^{-E/\mathcal{R}\tilde{T}}$$

where W_F, W_O are the molecular weights of the fuel and oxidizer, respectively and \mathcal{R} is the gas constant. The initial mixture strength representing the ratio of the fuel-to-oxidizer mass supplied in the respective boundaries, normalized by their stoichiometric proportion, is given by

$$\phi = \frac{\tilde{Y}_{F_0}/\tilde{Y}_{O_0}}{\nu_F W_F/\nu_O W_O}, \quad (1)$$

where \tilde{Y}_{F_0} and \tilde{Y}_{O_0} are the supplied fuel and oxidizer mass fractions.

The fuel and oxidizer supplied from opposing ends are appropriately diluted so that the mixture properties, such as mean molecular weight, thermal conductivity and

specific heat are determined by the abundant inert and the diffusivities $\tilde{\mathcal{D}}_F, \tilde{\mathcal{D}}_O$ are the fuel-inert and oxidizer-inert binary diffusivities, respectively. It is further assumed that the specific heat (at constant pressure) of the mixture c_p is constant, but the conductivity of the mixture $\tilde{\lambda}$ and the diffusion coefficients $\tilde{\mathcal{D}}_F, \tilde{\mathcal{D}}_O$ are temperature-dependent. Specifically $\tilde{\lambda}/c_p, \tilde{\rho}\tilde{\mathcal{D}}_F, \tilde{\rho}\tilde{\mathcal{D}}_O$ have the same temperature dependence such that the ratios $\text{Le}_F = \tilde{\lambda}/c_p\tilde{\rho}\tilde{\mathcal{D}}_F$ and $\text{Le}_O = \tilde{\lambda}/c_p\tilde{\rho}\tilde{\mathcal{D}}_O$, corresponding to the fuel and oxidizer Lewis numbers, remain constant.

2.1. Governing equations

For steady conditions, the mass flux $\tilde{m} = \text{const.}$ through the entire chamber. Conservation of energy of the mixture and the mass balance of the fuel and oxidizer are given by

$$\tilde{m}c_p \frac{d\tilde{T}}{d\tilde{x}} - \frac{d}{d\tilde{x}} \left(\tilde{\lambda} \frac{d\tilde{T}}{d\tilde{x}} \right) = Q\tilde{\omega}, \quad (2)$$

$$\tilde{m} \frac{d\tilde{Y}_i}{d\tilde{x}} - \frac{d}{d\tilde{x}} \left[\tilde{\rho}\tilde{\mathcal{D}}_i \left(\frac{d\tilde{Y}_i}{d\tilde{x}} + \alpha_{T_i} \frac{\tilde{Y}_i}{\tilde{T}} \frac{d\tilde{T}}{d\tilde{x}} \right) \right] = -\nu_i W_i \tilde{\omega}, \quad i = F, O \quad (3)$$

where the diffusion fluxes in (3) include the ordinary Fickian diffusion and the Soret thermal-diffusion transport effect, as appropriate for dilute mixtures. The adopted simplification is systematically derived from the Stefan-Maxwell relations in the Appendix. The subscript N used to identify the abundant inert in the binary diffusivity \mathcal{D}_{iN} , has been removed here for simplicity of notation. The thermal diffusion factor α_{T_i} is independent of the mixture composition and is treated as constant. Finally, the equation of state takes the form $\tilde{\rho}\tilde{T} = \tilde{\rho}_0\tilde{T}_0$, as appropriate for the near-isobaric conditions considered here.

To express the equations in dimensionless form, the state of the gas at $\tilde{x} = -L$ is used as reference: the temperature and density are made dimensionless with respect to \tilde{T}_0 and $\tilde{\rho}_0$, and the thermal diffusivity $\tilde{\mathcal{D}}_T = \tilde{\lambda}/\tilde{\rho}c_p$, and mass diffusivities of the fuel and oxidizer are scaled with respect to $\tilde{\mathcal{D}}_{T_0}, \tilde{\mathcal{D}}_{F_0}, \tilde{\mathcal{D}}_{O_0}$, respectively. Then,

$$\frac{\tilde{\lambda}}{\tilde{\lambda}_0} = \frac{\tilde{\rho}\tilde{\mathcal{D}}_F}{\tilde{\rho}_0\tilde{\mathcal{D}}_{F_0}} = \frac{\tilde{\rho}\tilde{\mathcal{D}}_O}{\tilde{\rho}_0\tilde{\mathcal{D}}_{O_0}} = \Lambda(T)$$

where $T = \tilde{T}/\tilde{T}_0$ is the dimensionless temperature. Typically, Λ obeys a power law with exponents in the range 0.5 – 1. We further choose L as the unit of length, and introduce the diffusion velocity $\tilde{\mathcal{D}}_{T_0}/L$ as a unit speed. The fuel and oxidizer mass fractions are normalized with respect to \tilde{Y}_{F_0} and \tilde{Y}_{O_1} , for convenience. The governing equations then become:

$$m \frac{dT}{dx} - \frac{d}{dx} \left(\Lambda \frac{dT}{dx} \right) = q\omega, \quad (4)$$

$$m \frac{dY_F}{dx} - \text{Le}_F^{-1} \frac{d}{dx} \left[\Lambda \left(\frac{dY_F}{dx} + \alpha_{T_F} \frac{Y_F}{T} \frac{dT}{dx} \right) \right] = -\omega, \quad (5)$$

$$m \frac{dY_O}{dx} - \text{Le}_O^{-1} \frac{d}{dx} \left[\Lambda \left(\frac{dY_O}{dx} + \alpha_{T_O} \frac{Y_O}{T} \frac{dT}{dx} \right) \right] = -\phi\omega, \quad (6)$$

where the dimensionless mass flux m is effectively the Peclet number, representing the ratio of convection to diffusion, and $q = Q\tilde{Y}_{F_0}/\nu_F W_F c_p \tilde{T}_0$ is the heat release parameter (the ratio of the heat release per unit mass of fuel and the enthalpy of the fresh mixture at temperature \tilde{T}_0). The reaction rate may be expressed in the form

$$\omega = \mathbb{D} T_s^2 \beta^3 \rho^2 Y_F Y_O \exp \left\{ \beta T_s \left(1 - \frac{T_s}{T} \right) \right\}, \quad (7)$$

where \mathbb{D} is the Damköhler number given by

$$\mathbb{D} = \frac{L^2}{\tilde{\lambda}_s / c_p} \left(\frac{\mathcal{R} \tilde{T}_s^2}{E \tilde{T}_0} \right)^3 \left(\frac{\tilde{\rho}_s}{\tilde{\rho}_0} \right)^2 \frac{\nu_O Y_{F_0}}{\phi W_F} \mathcal{B} e^{-E/\mathcal{R} \tilde{T}_s}, \quad (8)$$

where $\beta = E\tilde{T}_0/\mathcal{R}\tilde{T}_s^2$ is the activation energy parameter, \tilde{T}_s is the stoichiometric temperature, namely the temperature at the stoichiometric surface where the fuel and oxidizer meet in stoichiometric proportions and are completely consumed. Here and thereafter, when the same symbol is used the “tilde” accent denotes the dimensional (or normalized) quantity. The subscript s in $\tilde{\lambda}_s$ and $\tilde{\rho}_s$ has been used to indicate conditions at the stoichiometric surface. The modification of the exponential term, and the factor β^3 inserted in (7) are suggested by the asymptotic treatment for large activation energy ($\beta \gg 1$), which also requires that the Damköhler number be simultaneously large by means of a distinguished limit (8), as discussed in [5].

It should be noted that in Cheatham and Matalon [5], the term adiabatic flame temperature was used for the stoichiometric temperature \tilde{T}_s , noting that *it differs from the adiabatic flame temperature of a premixed combustible mixture because, for a diffusion flame, the flame temperature depends on the way in which the fuel and oxidant are brought together*. Thus, \tilde{T}_s depends in general on the Lewis numbers, as has been clearly demonstrated for the steady planar flame studied in the referenced paper [see Eq. (5.7), therein]. The term adiabatic flame temperature should more appropriately be reserved to the stoichiometric temperature when the fuel and oxidizer are supplied at the same temperature $\tilde{T}_0 = \tilde{T}_1$ and both Lewis numbers are equal to one, for then $\tilde{T}_s = \tilde{T}_a$ where

$$\tilde{T}_a = \tilde{T}_0 + \frac{Q\tilde{Y}_{F_0}/\nu_F W_F c_p}{1 + \phi}$$

is the adiabatic flame temperature of a mixture consisting of $\tilde{Y}_{F_0}/(1 + \phi)$ fuel and $\phi\tilde{Y}_{O_0}/(1 + \phi)$ oxidizer, at temperature \tilde{T}_0 . When the temperature at the two boundaries is not equal, the adiabatic, or stoichiometric temperature for unity Lewis numbers, includes the additional term $(\tilde{T}_1 - \tilde{T}_0)/(1 + \phi)$, which in dimensionless form, translates to

$$T_a = 1 + \frac{q + \Delta T}{1 + \phi}$$

where $\Delta T = (\tilde{T}_1 - \tilde{T}_0)/\tilde{T}_0$ is the (dimensionless) temperature differential between the values at the oxidizer and fuel boundaries. For nonunity Lewis numbers the stoichiometric temperature T_s depends on the flow configuration, as further elaborated below.

The boundary conditions in dimensionless form are

$$T = 1, Y_F = 1, Y_O = 0, \quad \text{at } x = -1, \quad (9)$$

$$T = 1 + \Delta T, Y_F = 0, Y_O = 1, \quad \text{at } x = 1, \quad (10)$$

The formulation consisting of (4)-(10) is valid for both cases: fuel supplied in the stream ($m > 0$) or oxidizer supplied in the stream ($m < 0$).

2.2. Activation Energy Asymptotics

For large activation energy, $\beta \gg 1$, the chemical reaction is confined to a sheet located at $x = x_f$ that divides the combustion field into two reaction-free regions: the fuel region corresponding to $-1 < x < x_f$, and the oxidizer region corresponding to $x_f < x < 1$. The resolution of the thin reaction zone, on the $\mathcal{O}(\beta^{-1})$ scale surrounding $x = x_f$, provides through asymptotic matching jump conditions for the state variables across the reaction sheet. The resulting free boundary problem can be deduced from the general formulation presented in Cheatham and Matalon [5] with minor modifications that arise from the additional Soret thermal diffusion fluxes and allowing the transport coefficients to be temperature-dependent. We note, however, that in rendering the equations dimensionless we have used a different scaling than the one used in [5], which led to the parameters q and ϕ appearing explicitly in the jump relations. The jump conditions across the reaction sheet, $x = x_f$, are

$$[[T]] = [[Y_F]] = [[Y_O]] = 0, \quad (11)$$

$$\frac{1}{q} [[\frac{dT}{dx}]] = -\frac{1}{\text{Le}_F} \left[\frac{dY_F}{dx} + \alpha_{T_F} \frac{Y_F}{T} \frac{dT}{dx} \right] = -\frac{1}{\phi \text{Le}_O} \left[\frac{dY_O}{dx} + \alpha_{T_O} \frac{Y_O}{T} \frac{dT}{dx} \right] \quad (12)$$

$$Y_F \Big|_{x_f^+} = \frac{\text{Le}_F}{q\beta} S_F(\gamma, \delta), \quad Y_O \Big|_{x_f^-} = \frac{\text{Le}_O}{q\beta} \phi S_O(\gamma, \delta), \quad (13)$$

where $[[\cdot]]$ denotes the jump operator, defined as the difference between the values of a quantity evaluated at x_f^+ and x_f^- .

Equation (11) affirms that all variables are continuous across the reaction sheet. Equation (12) states that the fuel and oxidizer flow into the reaction sheet from opposing sides in stoichiometric proportions, and the total energy released at the reaction sheet is conducted away at different rates that depend on the stoichiometric proportions. Equation (13) determines the extent of reactant leakage through the reaction zone in terms of the functions S_F and S_O that depend on two auxiliary parameters: the heat transfer parameter γ and the reduced Damköhler number δ . The parameter γ , given by

$$\gamma = \frac{dT/dx|_{x_f^+} + dT/dx|_{x_f^-}}{[[dT/dx]]}, \quad (14)$$

determines the excess of heat conducted to one side of the reaction sheet; it is positive when more heat is conducted towards the oxidizer side and negative when more heat is conducted towards the fuel side. For the diffusion-flame regime considered here,

$-1 < \gamma < 1$. The parameter δ is given by

$$\delta e^{-h_f(\gamma, \delta)} = \frac{4\phi \text{Le}_o \text{Le}_F}{q \llbracket dT/dx \rrbracket^2} \mathbb{D}, \quad (15)$$

determines the intensity of the chemical reaction where

$$h_f = \beta(T_f - T_s) + \frac{1 - \gamma}{2} S_F + \frac{1 + \gamma}{2} S_O,$$

where $h_f = h_f(\gamma, \delta)$ represents the excess enthalpy available at the reaction sheet, with T_f the flame temperature that differs from the stoichiometric temperature T_s due to incomplete combustion. It is evident that in order to satisfy the relations (11)-(13) the reaction-diffusion equations on either side of the reaction sheet need to be solved to $O(\beta^{-1})$ for the determination of h_f . Consequently, the relation (15) is, in general, an *implicit* nonlinear expression for δ .

The functional dependence of S_F and S_O on the parameters γ and δ , has been determined numerically [5] by solving the nonlinear boundary value problem that describes the internal structure of the thin reactive-diffusive zone. Due to the symmetry with respect to γ , the reactant leakage may be expressed as

$$S_F = \begin{cases} S_1 & 0 \leq \gamma < 1, \\ S_2 & -1 < \gamma \leq 0, \end{cases} \quad S_O = \begin{cases} S_2 & 0 \leq \gamma < 1, \\ S_1 & -1 < \gamma \leq 0, \end{cases} \quad (16)$$

where S_1 and S_2 are referred to as the leakage functions. Representative functions $S_1(\gamma, \delta)$ and $S_2(\gamma, \delta)$ are given in Fig. 2. The results show that for a given γ , two solutions exist for $\delta > \delta_c$ and none for $\delta < \delta_c$. An approximate expression for the critical value δ_c was first derived by Liñán [1] in the form

$$\delta_c = \{1 - |\gamma| - (1 - |\gamma|)^2 + 0.26(1 - |\gamma|)^3 + 0.055(1 - |\gamma|)^4\} e^1,$$

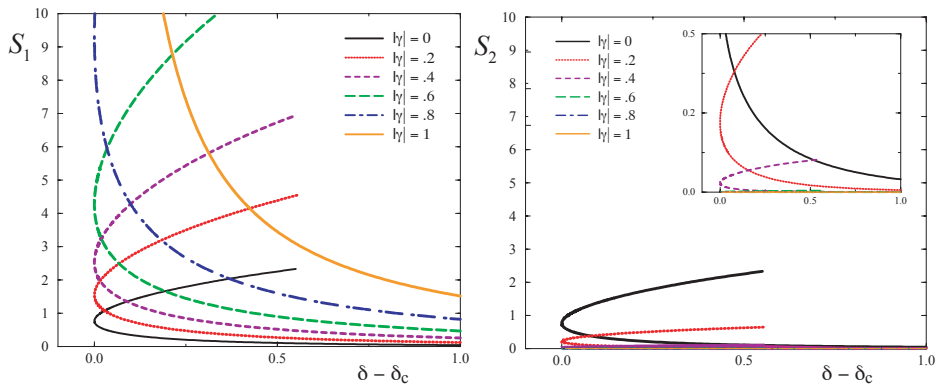


Figure 2: The leakage functions S_1 and S_2 as a function of $\delta - \delta_c$ for several values of γ .

and is found to represent the numerical values extremely well. The dependence of the leakage function on δ traces a C-shaped curve with a turning point at δ_c . The lower branch of the response curves is a monotonically decreasing function of δ that tends to zero when $\delta \rightarrow \infty$. The upper branch is a monotonically increasing function of δ that tends to infinity, or to a state associated with $\mathcal{O}(1)$ reactant leakage, when $\delta \rightarrow \infty$.

It is more appropriate to interpret these results in terms of the Damköhler number \mathbb{D} , which is controlled by the system parameters. When $\mathbb{D} \rightarrow \infty$, both reactants are completely consumed; the reaction sheet separates a region where there is fuel but no oxidizer from a region where there is only oxidizer, as originally envisioned by Burke and Schumann [15], and its temperature reaches the stoichiometric temperature T_s . When systematically decreasing \mathbb{D} , there is a continuous increase in reactant leakage through the reaction sheet and an associated drop in flame temperature T_f . This behavior persists until $\mathbb{D} = \mathbb{D}_{\text{ext}}$, which marks the value below which a steady flame can no longer be sustained due to insufficient mixing and a low temperature. Because of the nonlinear dependence of the Damköhler number on δ exhibited in (15), the extinction state \mathbb{D}_{ext} does not necessarily coincide with the critical δ_c . The extinction state \mathbb{D}_{ext} lies on the lower branch of the leakage response curve when $h_f < 0$, and on the upper branch of the leakage response curve when $h_f > 0$. In general, the upper branch of the response curves is of limited physical interest, corresponding typically to unstable states [16, 17]. The aforementioned asymptotic formulation, therefore, covers the entire range from complete combustion to extinction.

In order to have direct access to the leakage functions, without the necessity to repeatedly integrate numerically the boundary value problem, Cheatham and Matalon [5] provided the following formulae

$$S_1 = \begin{cases} \delta^{-1/3} \{q_0 + q_1(\delta - \delta_c)^{q_2}\} & \text{upper branch,} \\ a_0 \delta^{-4/3} \exp\{-a_1(\delta - \delta_c)^{a_2}\} & \text{lower branch,} \end{cases}$$

$$S_2 = \begin{cases} \delta^{-1/3} \{r_0 + r_1(\delta - \delta_c)^{r_2}\} & \text{upper branch,} \\ b_0 \delta^{-4/3} \exp\{-b_1(\delta - \delta_c)^{b_2}\} & \text{lower branch;} \end{cases}$$

which were shown to represent the numerical results with sufficient accuracy. The coefficients a_k , b_k , q_k , and r_k for $k = 0, 1, 2$, that depend only on $|\gamma|$, can be found in [5] and will not be repeated here.

The modification in the asymptotic formulation that resulted from allowing the diffusivities to vary with temperature, appear in (8), where $\tilde{\lambda}$ has been replaced by its value at the reaction sheet, namely $\tilde{\lambda}_s = \tilde{\lambda}(\tilde{T}_s)$. Since $\Lambda(T)$ is continuous across the reaction sheet, no change are observed in the jump relations (12). The other modification to the formulation appears in the jump relations (12) where the net flux of reactants flowing into the reaction sheet account now for the additional Soret transport. These relations can be directly deduced by integrating the appropriate combinations of equations (4)-(6) across the reaction sheet, but can be also obtained as matching conditions if one reexamines the internal structure of the reaction sheet following [5] (the details that we do not show here). Finally, since $Y_F, Y_O \sim \mathcal{O}(\beta^{-1})$ at the reaction sheet, the Soret effect is also an $\mathcal{O}(\beta^{-1})$ effect that becomes more pronounced near the extinction conditions where there is a significant reactant leakage through the reaction sheet.

In the proceeding sections the effect of variable transport properties and Soret effect on the characteristics of the reaction sheet are examined separately. First variable transport properties with no Soret effect is examined for two cases, the Burke-Schumann limit (with comparison to experimental data) and incomplete combustion. Then the Soret effect with constant transport properties is also analyzed for the Burke-Schumann limit and then incomplete combustion.

3. Variable Transport

The system of equations (4)-(13) for $\alpha_T^i = 0$ has a solution corresponding to a planar flame with the temperature and mass fractions profiles given by

$$T = \begin{cases} 1 + (T_f - 1) \frac{e^{F(x)} - 1}{e^{F(x_f)} - 1} & -1 < x < x_f, \\ 1 + \Delta T + (T_f - 1 - \Delta T) \frac{e^{-G(x)} - 1}{e^{-G(x_f)} - 1} & x_f < x < 1, \end{cases} \quad (17)$$

$$Y_F = \begin{cases} 1 - (1 - \beta^{-1} q^{-1} \text{Le}_F S_F) \frac{e^{\text{Le}_F F(x)} - 1}{e^{\text{Le}_F F(x_f)} - 1} & -1 < x < x_f, \\ \beta^{-1} q^{-1} \text{Le}_F S_F \frac{e^{-\text{Le}_F G(x)} - 1}{e^{-\text{Le}_F G(x_f)} - 1} & x_f < x < 1, \end{cases} \quad (18)$$

$$Y_O = \begin{cases} \beta^{-1} q^{-1} \phi \text{Le}_O S_O \frac{e^{\text{Le}_O F(x)} - 1}{e^{\text{Le}_O F(x_f)} - 1} & -1 < x < x_f, \\ 1 - (1 - \beta^{-1} q^{-1} \phi \text{Le}_O S_O) \frac{e^{-\text{Le}_O G(x)} - 1}{e^{-\text{Le}_O G(x_f)} - 1} & x_f < x < 1, \end{cases} \quad (19)$$

where

$$F(x) = \int_{-1}^x \frac{m}{\Lambda} d\tilde{x}, \quad \text{and} \quad G(x) = \int_x^1 \frac{m}{\Lambda} d\tilde{x}.$$

The solution includes expressions for the location of the reaction sheet $x = x_f$ and the flame temperature $T_f = T(x_f)$. Since the asymptotic model is correct to $\mathcal{O}(\beta^{-2})$, these must be expressed in the form $x_f = \eta_0 + \beta^{-1}\eta_1 + \dots$ and $T_f = T_s + \beta^{-1}T_{f1} + \dots$. The leading terms can be easily computed; the location of the reaction sheet (the stoichiometric surface, in this case) results from

$$\frac{1 - e^{-\text{Le}_F F_0}}{1 - e^{\text{Le}_O G_0}} = -\phi, \quad (20)$$

and the stoichiometric temperature is given by

$$T_s = 1 + \Delta T \frac{e^{-G_0} (e^{F_0} - 1)}{e^{F_0} - e^{-G_0}} - q \frac{e^{\text{Le}_F F_0} (e^{F_0} - 1) (e^{-G_0} - 1)}{(e^{\text{Le}_F F_0} - 1) (e^{F_0} - e^{-G_0})},$$

where F_0 and G_0 denote $F(\eta_0)$ and $G(\eta_0)$ respectively. The $\mathcal{O}(\beta^{-1})$ terms can be written explicitly, but they involve cumbersome relations that will not be given here. For unity Lewis numbers the stoichiometric flame temperature reduces to

$$T_s = q + 1 + (\Delta T - q)(1 + \phi^{-1})^{-1}.$$

This is the flame temperature to leading order as seen in Cheatham and Matalon [5], using the scaling of this paper, and is regardless of temperature dependent or constant transport properties. It can be shown numerically that for generic Lewis numbers the stoichiometric flame temperature is the same for temperature dependent and constant transport properties. In Fig. 3 the effect of Lewis numbers on the stoichiometric flame temperature is given for both the temperature dependent and constant transport properties with $m = 1$. As both Lewis numbers decrease, the diffusivity of the reactants increase, and the flame temperature increases. When the fuel is in the flow $m > 0$, and Le_O changes then there is no difference between the flame temperature for constant and temperature dependent transport. The flame temperature is smaller for the temperature dependent versus constant transport properties when $Le_F > 0$.

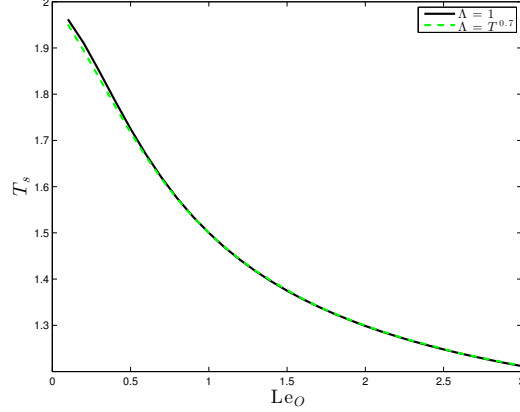
The entire analytical solution (17)-(19) appears in an implicit form because the integrals that constitute $F(x)$ and $G(x)$ depend on the temperature T over entire intervals and the location of the reaction sheet x_f that also depends on the temperature T . However, for constant transport ($\Lambda = 1$), $F = m(x + 1)$, $G = -m(1 - x)$ and (17)-(19) are explicit functions for the determination of T, Y_F, Y_O , that depend on x_f and must be first determined from (20).

Presenting the results for variable transport, necessitates using an iterative numerical scheme. A convenient initial guess is the solution for complete combustion ($\beta^{-1} = 0$) with constant transport properties ($\Lambda = 1$), which can be written explicitly. For the results presented below we assume that $\Lambda = T^n$ with $n = 0.7$. Varying n in the range $0.5 \leq n \leq 1$ produce results that do not differ significantly from those with $n = 0.7$. Furthermore, for simplicity, we consider the case when there is no temperature difference between the two boundaries, $\Delta T = 0$.

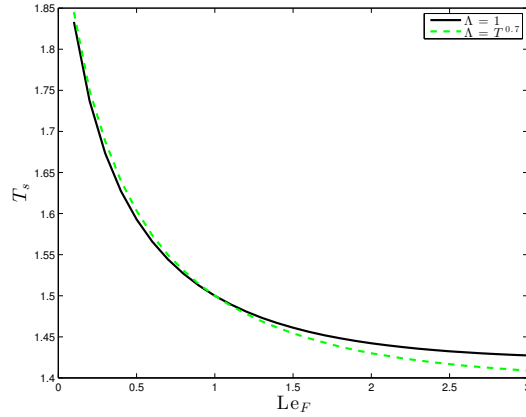
3.1. Burke-Schumann Limit

The Burke-Schumann limit (complete combustion) is obtained by setting $\beta^{-1} = 0$. Figure 4(a) shows temperature and the mass fraction profiles across the entire chamber, with constant and variable transport for the case in which the bulk flow is directed to the reaction zone from the fuel side. Figure 4(b) shows similar profiles, but for the reverse case, namely when the bulk flow is directed towards the reaction zone from the oxidizer side. These graphs clearly identify the influence that temperature-dependent transport coefficients has on the flame structure. We first note that with variable transport, the reaction sheet (or stoichiometric surface) shifts towards the fuel boundary when the direction of the bulk flow is from the fuel side ($m > 0$), and towards the oxidizer boundary when the bulk flow is from the oxidizer side ($m < 0$).

As a result, it is clear that at any position x the fuel mass fraction Y_F will be smaller, and the oxidizer mass fraction Y_O larger, when $\Lambda = \Lambda(T)$ than when $\Lambda = 1$. Another observation is that the stoichiometric flame temperature is unaffected by whether Λ depends on temperature or not (this appears to be a general result). Consider first



(a) $Le_F = 1.0, \phi = 1.00$

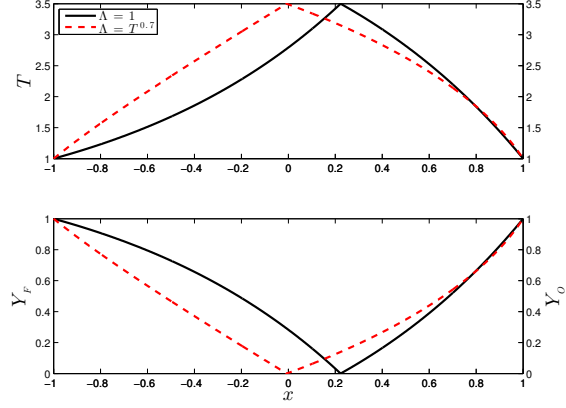


(b) $Le_O = 1.0, \phi = 1.00$

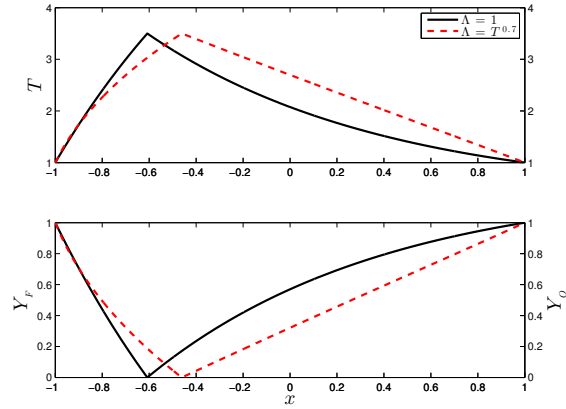
Figure 3: The stoichiometric flame temperature, T_s as a function of Lewis numbers for constant (solid curve), temperature-dependent (dashed curve) transport.

$m > 0$; since the temperature at the reaction sheet and at the two boundaries $x = \pm 1$ are held fixed, the temperature profile on the fuel side will necessarily be larger with variable than with constant transport, and will be smaller on the oxidizer side. The reverse is true when $m < 0$.

The location of the reaction sheet, or stoichiometric surface, is solely determined by the fuel and oxidizer fluxes that must flow into the reaction sheet in stoichiometric proportions. Therefore x_f must depend on the initial mixture strength ϕ and the fuel and oxidizer diffusivities $\mathcal{D}_F, \mathcal{D}_O$; respectively. The limit $m = 0$ is particularly instructive; it corresponds to an ideal diffusion flame where both reactants reach the reaction zone purely by diffusion. An expression for the stoichiometric surface η_0 in this case can be obtained from (20) using L'Hôpital's Rule and integrating the corresponding



(a) Bulk flow directed towards the reaction sheet from the fuel side.



(b) Bulk flow directed towards the reaction sheet from the oxidizer side.

Figure 4: Temperature and mass fraction profiles with constant (solid curves) and temperature-dependent (dashed curve) transport for (a) $m = 1$ and (b) $m = -1$. Calculated for $\phi = 0.6$, unity Lewis number, $q = 4.0$, and $T_0 = 1$.

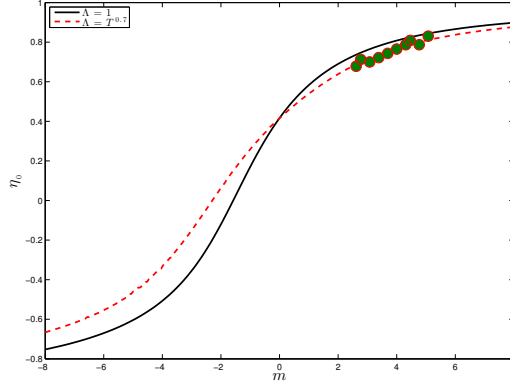
temperature profile, which yields

$$\eta_0 = \frac{\Phi - 1}{\Phi + 1}, \quad (21)$$

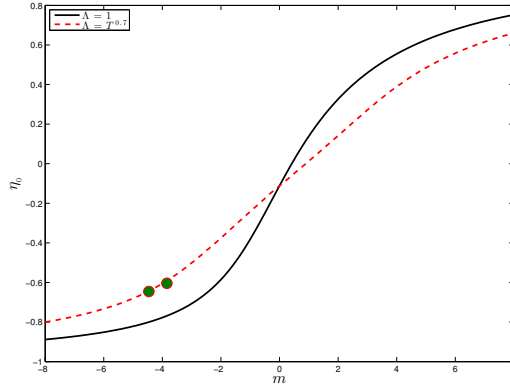
where

$$\Phi = \frac{\text{Le}_O}{\text{Le}_F} \phi = \frac{\tilde{Y}_{F_0}/\nu_F W_F}{\tilde{Y}_{O_1}/\nu_O W_O} \cdot \frac{\mathcal{D}_F}{\mathcal{D}_O},$$

that may be considered as the “effective mixture strength”. This depends not only on the ratio of the initial mass of fuel and oxidizer, but also on the ratio of their diffusivi-



(a) $Le_F = 0.35, Le_O = 0.85, \phi = 1$



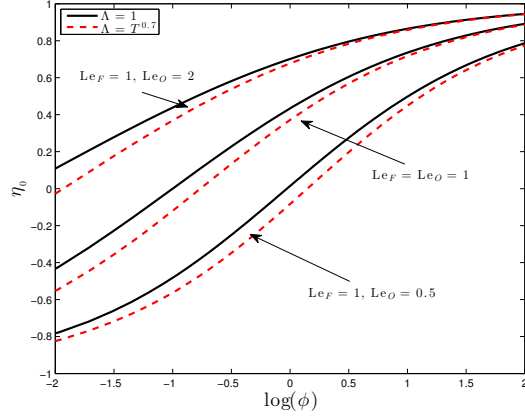
(b) $Le_F = 0.25, Le_O = 0.80, \phi = 0.25$

Figure 5: The location of the stoichiometric surface η_0 for complete combustion as a function of the bulk flow velocity for constant (solid curve), temperature-dependent (dashed curve) transport, and solid circles of experimental data obtained from [13].

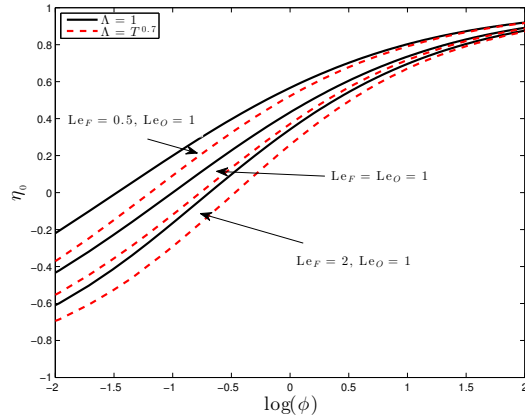
ties. When fuel and oxidizer are supplied in stoichiometric proportions and there is no preferential diffusion, the problem is completely symmetric and $\eta_0 = 0$. This result is true whether Λ depends on temperature or not. The corresponding flame temperature to leading order is

$$T_s = T_0 + \frac{q}{Le_F + Le_O \phi},$$

where the temperature difference (ΔT) is zero. As the diffusivity of the fuel and oxidizer increase (the Lewis numbers decrease) the stoichiometric flame temperature increases. Since for $m > 0$ the oxidizer diffuses against the stream, the reaction sheet is located near the oxidizer boundary; when the diffusivity increases with temperature the ability of oxidizer to penetrate the stream is enhanced, resulting in a smaller value



(a) Variation in oxidizer Lewis number Le_O

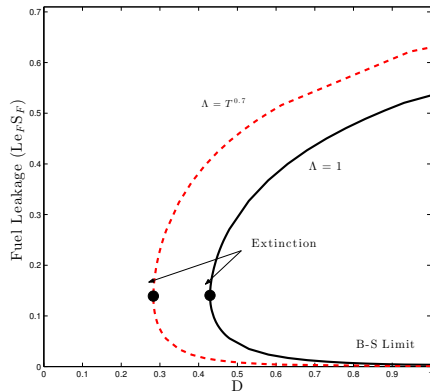


(b) Variation in fuel Lewis number Le_F

Figure 6: The location of the reaction sheet as a function of the initial mixture strength ϕ for constant (solid curve) and variable (dashed curve) transport. Calculated for $m = 1, T_0 = 1$.

of η_0 . For $m < 0$ it is the fuel that diffuses against the stream and the reaction sheet is near the fuel boundary; but when the diffusivity depends on temperature the fuel is more mobile which results in a larger value of η_0 .

In Fig. 5 we show the dependence of η_0 on the magnitude and direction of the bulk flow for two sets of conditions, and compare the results to those obtained from the experimental data of Robert and Monkewitz [13] and [18]. In Fig. 5(a) the conditions correspond to $\Phi > 1$ and the reaction sheet for $m = 0$ is located on the oxidizer side, at $\eta_0 = 0.4$. In Fig. 5(b) the conditions correspond to $\Phi < 1$ and the reaction sheet for $m = 0$ is located on the oxidizer side, at $\eta_0 = -0.16$. When there is a bulk flow, the trend for constant and variable transport follow the discussion presented above. These results are in agreement with the experimental data of Robert and Monkewitz [18].



(a) $\phi = 0.6$

Figure 7: Response curves showing the extent of fuel leakage on \mathbb{D}_0 , for various values of the initial mixture strength ϕ , for constant (solid curve) and variable (dashed curve) transport coefficients. Calculated for unity Lewis numbers.

Figure 6 gives an example of the the dependence of η_0 on the initial mixture strength for different sets of Lewis numbers. We note that the effect of increasing Le_O on the location η_0 is more significant then the effect of increasing Le_F ; this is because the flow is directed from the fuel side and oxidizer diffuses against the stream. The opposite trend is seen when $m < 0$.

3.2. Incomplete Combustion

The Burke-Schumann limit of complete combustion results when $\delta \rightarrow \infty$, and since δ is inversely proportional to m^2 so that at low flow rates it allows for simultaneous mixing and chemical reaction. At higher flow rates, there may be incomplete combustion, the flame temperature T_f is reduced to below the stoichiometric temperature T_s and there is an $\mathcal{O}(\epsilon)$ leakage of fuel and/or oxidizer through the reaction sheet. The leakage increases as m increases, and beyond a critical value a steady flame can no longer be sustained in the chamber. These conditions are associated with extinction and can be identified as a turning point when plotting the reactant leakage as a function of the effective Damköhler number \mathbb{D} . Figure 7 shows the fuel leakage as a function of the effective Damköhler number for several values of ϕ , for constant as well as variable transport. The results clearly show that by appropriately accounting for the temperature dependence in the transport coefficients, the critical Damköhler number is lower than the value estimated with constant coefficients.

4. Thermal-diffusion (Soret-effect)

The system of equations (4)-(13) for $\Lambda(T) = 1$ and for Soret effect only in the fuel $\alpha_{T_O} = 0$, has a solution corresponding to a planar flame with the temperature and mass

fractions profiles given by

$$T = \begin{cases} 1 + (T_f - 1) \frac{e^{m(x+1)} - 1}{e^{m(x_f+1)} - 1} & -1 < x < x_f, \\ 1 + \Delta T + (T_f - 1 - \Delta T) \frac{e^{m(x-1)} - 1}{e^{m(x_f-1)} - 1} & x_f < x < 1 \end{cases} \quad (22)$$

$$Y_O = \begin{cases} \beta^{-1} q^{-1} \text{Le}_O \phi S_O \frac{e^{m\text{Le}_O(x+1)} - 1}{e^{m\text{Le}_O(x_f+1)} - 1} & -1 < x < x_f, \\ 1 - (1 - \beta^{-1} q^{-1} \text{Le}_O \phi S_O) \frac{e^{m\text{Le}_O(x-1)} - 1}{e^{m\text{Le}_O(x_f-1)} - 1} & x_f < x < 1 \end{cases} \quad (23)$$

$$Y_F = \begin{cases} e^{m\text{Le}_F(x+1)} T^{-\alpha_T} \left[1 - \frac{A(x)}{A(x_f)} \right] + \beta^{-1} q^{-1} \text{Le}_F S_F e^{m\text{Le}_F(x-x_f)} \left(\frac{T_f}{T} \right)^{\alpha_T} \frac{A(x)}{A(x_f)} & -1 < x < x_f, \\ \beta^{-1} q^{-1} \text{Le}_F S_F e^{m\text{Le}_F(x-x_f)} \left(\frac{T_f}{T} \right)^{\alpha_T} \frac{B(x)}{B(x_f)} & x_f < x < 1 \end{cases} \quad (24)$$

where

$$A(x) = \int_{-1}^x e^{-m\text{Le}_F \tilde{x}} T^{\alpha_T} d\tilde{x}, \quad \text{and} \\ B(x) = \int_x^1 e^{-m\text{Le}_F \tilde{x}} T^{\alpha_T} d\tilde{x}. \quad (25)$$

The location of the flame front is found to be a transcendental equation for x_f and T_f . The model is only correct to $\mathcal{O}(\epsilon^2)$ so we expand $x_f = \eta_0 + \epsilon\eta_1 + \dots$, and $T_f = T_s + \epsilon T_{f1} + \dots$ to leading order

$$-\phi = \frac{m\text{Le}_F A_0}{e^{m\text{Le}_F} (1 - e^{-m\text{Le}_O(\eta_0-1)})} \quad (26)$$

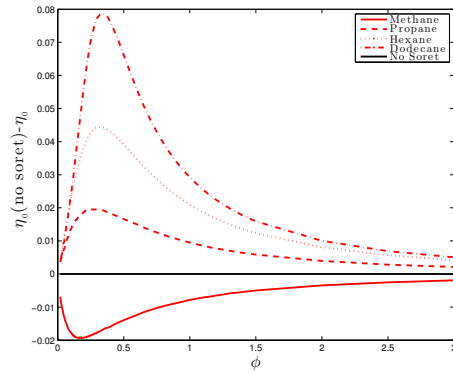
and

$$T_s = 1 + \Delta T \frac{e^{m(\eta_0+1)} - 1}{e^{2m} - 1} + \frac{q}{\phi} \frac{e^{-m\eta_0} (e^{m(\eta_0+1)} - 1) (e^{m(\eta_0-1)} - 1)}{(e^m - e^{-m}) (1 - e^{-m\text{Le}_O(\eta_0-1)})} \quad (27)$$

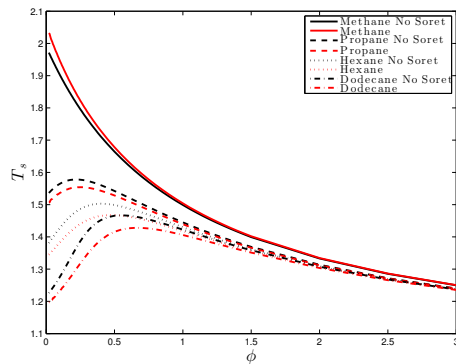
where $A_0 = A(\eta_0)$. The $\mathcal{O}(\epsilon)$ terms can be written explicitly, but will not be written here.

The numerical scheme to solve for the location of the reaction sheet is the same as what was done in the Variable Transport - No Soret Effect section. We examine Soret effect for several types of fuels given in table 1 of the appendix. To simplify the graphs the value of nonane was not used, but the trends discussed below are consistent for nonane as well.

For the Burke-Schumann solution (complete combustion) when $\beta^{-1} = 0$, Fig. 8(a) shows the difference between the location of the reaction sheet for no-Soret diffusion and Soret diffusion for dodecane, hexane, propane, and methane as a function of ϕ . For



(a) Difference in the location of the reaction sheet as a function of ϕ .

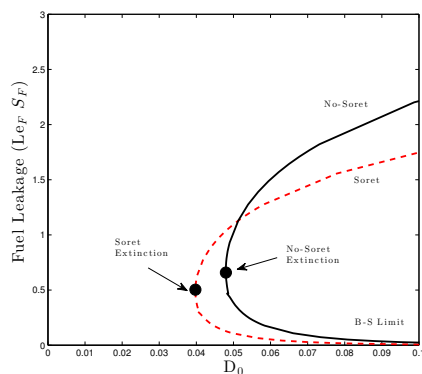


(b) Stoichiometric temperature as a function of ϕ

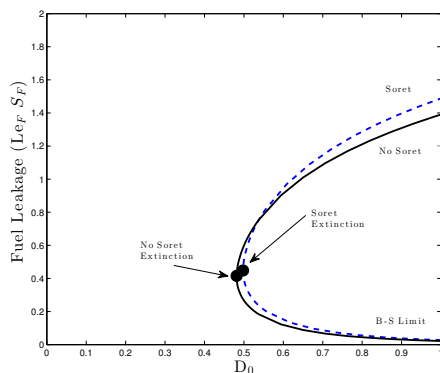
Figure 8: Calculations for α_T and Le_F are taken from Table 1 and $Le_O = 1$, $m = 1$, and $T_0 = 1$. Note: nonane was not used, this was done to keep the graphs readable.

the heavy fuel the location of the reaction sheet shifts towards the fuel region, as the fuel decreases in size the difference between including Soret and not including Soret decreases. For the case of light fuel like methane the reaction sheet shifts toward the oxidizer region. Figure 8(b) shows the stoichiometric temperature as a function of ϕ for dodecane, hexane, propane, and methane. The stoichiometric temperature is smaller for dodecane and as the fuel becomes smaller the difference in the stoichiometric temperature while including Soret effects and not including Soret effects becomes smaller. For the light fuel of methane the stoichiometric temperature is larger when accounting for Soret effects. Figure 8 is in agreement with the results given by Arias-Zugasti and Rosner [11].

The conditions under which extinction happens is examined for both a heavy fuel (dodecane) and a light fuel (methane) in Fig. 9. In Fig. 9(a) the response curve for



(a) Response curve for dodecane; Soret diffusion (dashed curve) and no-Soret (solid curve).



(b) Response curve for methane; Soret diffusion (dashed curve) and no-Soret (solid curve)

Figure 9: Calculations made for dodecane (a) were $\alpha_T = 1.4$ and $Le_F = 4.63$ and methane (b) were $\alpha_T = -0.17$ and $Le_F = 1.01$; and $\phi = 0.8$, $Le_O = 1$, and $T_0 = 1$.

dodecane with Soret diffusion shows that a smaller amount of leakage leads to extinction. The opposite trend is seen for methane, Fig. 9(b), in which a larger amount of leakage is required for extinction. In both cases there is a slight difference in the amount of flow for extinction.

5. Conclusion

The planar chambered flame was used to investigate the influence of temperature-dependent transport properties and Soret diffusion on the structure of a diffusion flame. The results for the temperature-dependent transport properties show a significant change

in the location of the reaction sheet, particularly when one of the reactants has to diffuse against a relatively strong flow. The stoichiometric flame temperature is not affected by temperature-dependent transport; however the correction to the flame temperature due to incomplete combustion does change when variations in thermal and mass diffusivities with temperature are accounted for. Furthermore, it was found that when assuming constant transport properties the extinction conditions identified by a critical Damköhler number \mathbb{D}_c below which a steady flame may not be sustained are overestimated. The critical Damköhler number \mathbb{D}_c when transport properties are more realistically modeled is significantly lower. Finally, predictions with temperature-dependent transport properties better approximate the location of the reaction sheet and the profiles of the reactants when compared to experimental data from Robert and Monkewitz [18].

Also both heavy and light fuels were investigated to see the implications of including Soret effect in the analysis of diffusion flames. Motivated by estimates of the thermal diffusion coefficients, the Soret effect was only included in the diffusion flux relation for the fuel equations where the oxidizer was assumed to follow a Fickian's law. Since the reaction zone is essentially a diffusive-reactive zone, its internal structure of the reaction sheet was re-analyzed with the inclusion of Soret effect, using the same analysis of Cheatham and Matalon [5]. The modifications to the jump in the flux conditions across the reaction sheet due to the Soret effect were found to be relatively small and on the order $O(\beta^{-1})$. Results show that several flame characteristics are affected by thermal diffusion. The location of the reaction sheet and the stoichiometric temperature see a slight change especially when there is a very heavy fuel such as dodecane or a very light fuel such as methane. These results are in agreement with those of Arias-Zugasti and Rosner [11]. In this work it has been observed, that due to thermal diffusion, that a smaller amount of leakage through the reaction zone for heavy fuels and a larger amount of leakage is necessary for light fuels for extinction to occur.

Appendix A

The multi-component Stefan-Maxwell equation [19] for a mixture comprising of N species, neglecting body and pressure forces, is

$$\nabla X_i = \sum_{j=1}^N \frac{X_i X_j}{\mathcal{D}_{ij}} (\mathbf{V}_j - \mathbf{V}_i) + \frac{X_i X_j}{\rho \mathcal{D}_{ij}} \left(\frac{\mathcal{D}_j^T}{Y_j} - \frac{\mathcal{D}_i^T}{Y_i} \right) \frac{\nabla T}{T}, \quad (28)$$

where \mathbf{V}_i is the diffusion velocity, X_i the molar fraction, Y_i the mass fraction of species i , and $\mathcal{D}_{ij}, \mathcal{D}_i^T$ are the binary diffusivities and thermal diffusion coefficients respectively. The mass and molar fractions satisfy

$$\sum_{j=1}^N X_j = 1, \quad \sum_{j=1}^N Y_j = 1, \quad (29)$$

and are related via $Y_i = X_i W_i / W$, where W_i is the molecular weight of species i and

$$W = \sum_{j=1}^N X_j W_j, \quad (30)$$

the average molecular weight of the mixture. An additional constrain is

$$\sum_{j=1}^N Y_j \mathbf{V}_j = 0. \quad (31)$$

stating that the net diffusion mass flux is zero.

For a dilute mixture, all species are scarce relative to an abundant diluent, identified as species N . Then $X_i \ll 1$ and $Y_i \ll 1$ for $i = 1, \dots, N-1$, while $Y_N \sim 1$ and $X_N \sim 1$. Consequently, (31)-(30) imply that $V_N \ll 1$ and $W \sim W_N$, such that $Y_i = X_i W_i / W_N$. With these simplifications the Stefan-Maxwell equation (28) reduces to

$$\nabla X_i \sim -\frac{X_i \mathbf{V}_i}{\mathcal{D}_{iN}} - \frac{X_i}{Y_i} \frac{D_i^T}{\rho \mathcal{D}_{iN}} \frac{\nabla T}{T}, \quad i=1, \dots, N-1 \quad (32)$$

and, when expressed in terms of the mass fractions, yields an explicit expression for the diffusion mass flux

$$\rho Y_i \mathbf{V}_i = -\rho \mathcal{D}_{iN} \nabla Y_i - \mathcal{D}_i^T \frac{\nabla T}{T}, \quad i=1, \dots, N-1. \quad (33)$$

The thermal diffusion ratio k_i^T , is commonly defined [20] as

$$k_i^T = \frac{\rho}{C^2 W_i W_N} \frac{\mathcal{D}_i^T}{\mathcal{D}_{iN}},$$

where $C_i = \rho Y_i / W_i$, is the concentration of species i and C is the total concentration. For dilute mixtures, $C \sim \rho / W_N$ and $k_i^T = (W_N / \rho W_i) (\mathcal{D}_i^T / \mathcal{D}_{iN})$. This coefficient, however, depends on the mixture composition, while the (dimensionless) thermal diffusion factor $\alpha_{T_i} \equiv k_i^T / X_i X_N$ is nearly constant [10]. Introducing $\mathcal{D}_i^T \sim \rho Y_i \mathcal{D}_{iN} \alpha_{T_i}$ into (33), yields

$$\rho Y_i \mathbf{V}_i = -\rho \mathcal{D}_{iN} \left(\nabla Y_i + \alpha_{T_i} Y_i \frac{\nabla T}{T} \right), \quad i=1, \dots, N-1. \quad (34)$$

The equivalent expression for $i = N$ is rather complicated, involving on its right hand side a summation over all species. This expression, however, is not needed because it will only appear in the mass balance equation of species N , and Y_N can be obtained instead from the constrain (29) once all the other mass fractions have been determined.

Equation (34) is an explicit expression for the diffusion mass flux of species i , in a mixture dominated by an inert N . The first term on the right hand side is Fick's law of diffusion, whereby mass is transported from high-to-low concentration regions with coefficient \mathcal{D}_{iN} corresponding to the binary diffusivity of the representative species

and the abundant inert. The second term results from a temperature gradient with coefficient $\mathcal{D}_{iN} \alpha_{T_i}$ corresponding to thermal diffusion or Soret diffusivity. When $\alpha_{T_i} > 0$, species i moves towards the colder region, and when $\alpha_{T_i} < 0$, species i moves towards the warmer region. Representative values of α_T are shown in Table 1 for selective fuels. We note that $\alpha_T > 0$ for heavy fuels and $\alpha_T < 0$ for light fuels.

Compound	W_F	α_T	Le
Methane	16.04	-0.17	1.01
Propane	44.10	0.24	1.90
Hexane	86.17	0.64	2.71
Nonane	128.25	1.08	3.85
Dodecane	170.23	1.4	4.63

Table 1: Values for the thermal diffusion factor α_{T_F} and the corresponding Lewis number for representative fuels; taken from Rosner [9]. Note the definition of the Lewis number is the conventional one used in the combustion literature, which is the reciprocal of the Lewis number defined in Rosner's [9] text.

References

- [1] A. Liñán, The asymptotic structure of counterflow diffusion flames for large activation energies, *Acta Astronautica* 2 (1974) 1009.
- [2] M. Matalon, G. Ludford, J. Buckmaster, Diffusion flames in a chamber, *Acta Astronautica* 6 (1979) 943–959.
- [3] S. Chung, C. Law, Structure and Extinction of Convective Diffusion Flames with General Lewis Numbers, *Combustion and Flame* 52 (1983) 59–79.
- [4] J. Kim, F. Williams, Extinction of diffusion flames with nonunity Lewis numbers, *Journal of Engineering Mathematics* 31 (1997) 101–118.
- [5] S. Cheatham, M. Matalon, A general asymptotic theory of diffusion flames with application to cellular instability, *Journal of Fluid Mechanics* 414 (2000) 105–144.
- [6] C. K. Law, H. K. Law, Quasi-steady diffusion flame theory with variable specific heats and transport coefficients, *Combustion Science and Technology* 12 (1976) 207–216.
- [7] I. K. Puri, P. A. Libby, The influence of transport properties on droplet burning, *Combustion Science and Technology* 76 (1991) 67–80.
- [8] J. Warnatz, U. Maas, R. Dibble, *Combustion*, Springer-Verlag, Heidelberg, Germany, 1996.
- [9] D. E. Rosner, *Transport Processes in Chemically Reacting Flow Systems*, Dover Publications, Mineola, N.Y. (Second Edition) 2000., Dover Publications, Mineola, N.Y., second edition edn., 2000.
- [10] D. Rosner, R. Israel, B. La Mantia, Heavy species Ludwig-Soret transport effects in air-breathing combustion, *Combustion and Flame* 123 (2000) 547–560.
- [11] M. Arias-Zugasti, D. E. Rosner, Soret transport, unequal diffusivity, and dilution effects on laminar diffusion flame temperatures and positions, *Combustion and Flame* 153 (2008) 33–44.
- [12] D. Lo Jacono, P. Papas, M. Matalon, P. Monkewitz, An experimental realization of an unstrained planar diffusion flame, *Proceedings of the Combustion Institute* 30 (2005) 501–509.
- [13] E. Robert, P. Monkewitz, Experiments in a novel quasi-1D diffusion flame with variable bulk flow, *Proceedings of the Combustion Institute* 32 (2009) 987–994.
- [14] E. Robert, P. Monkewitz, Experimental realization and characterization of unstretched planar one-dimensional diffusion flames, *Combustion and Flame* 159 (1228-1238).

- [15] S. Burke, T. Schumann, Diffusion flames, *Industrial and Engineering Chemistry* 20 (1928) 998.
- [16] P. Metzner, M. Matalon, Diffusive-Thermal Instabilities of Diffusion Flames: Onset of Cells and Oscillations, *Combustion Theory and Modelling* 10 (4) (2006) 701–725.
- [17] M. Matalon, P. Metzner, The effect of thermal expansion on diffusion flame instabilities, *Journal of Fluid Mechanics* 647 (2010) 453–472.
- [18] E. Robert, P. Monkewitz, Thermal-diffusive instabilities in unstretched, planar diffusion flames, *Combust. Flame* 159 (2012) 1228–1238.
- [19] J. Hirschfelder, C. Curtiss, R. Bird, *Molecular Theory of Gases and Liquids*, John Wiley and Sons, New York, NY, 1967.
- [20] R. B. Bird, W. E. Stewart, E. N. Lightfoot, *Transport Phenomena*, John Wiley and Sons, New York, N.Y., 2001.